Environ. Sci. Technol. **2010,** *44,* 612–617

Molecular Scale Assessment of Methylarsenic Sorption on Aluminum Oxide

MASAYUKI SHIMIZU,* MATTHEW GINDER-VOGEL, SANJAI J. PARIKH,† AND DONALD L. SPARKS

Department of Plant and Soil Sciences, Delaware Environmental Institute, University of Delaware, Newark, Delaware 19716

Received September 10, 2009. Revised manuscript received November 26, 2009. Accepted December 1, 2009.

Methylated forms of arsenic (As), monomethylarsenate (MMA) and dimethylarsenate (DMA), have historically been used as herbicides and pesticides. Because of their large application to agriculture fields and the toxicity of MMA and DMA, the sorption of methylated As to soil constituents requires investigation. MMA and DMA sorption on amorphous aluminum oxide (AAO) was investigated using both macroscopic batch sorption kinetics and molecular scale extended X-ray absorption fine structure (EXAFS) and Fourier transform infrared (FTIR) spectroscopic techniques. Sorption isotherm studies revealed sorption maxima of 0.183, 0.145, and 0.056 mmol As/mmol Al for arsenate (As^V), MMA, and DMA, respectively. In the sorption kinetics studies, 100% of added As^V was sorbed within 5 min, while 78% and 15% of added MMA and DMA were sorbed, respectively. Desorption experiments, using phosphate as a desorbing agent, resulted in 30% release of absorbed As^V, while 48% and 62% of absorbed MMA and DMA, respectively, were released. FTIR and EXAFS studies revealed that MMA and DMA formed mainly bidentate binuclear complexes with AAO. On the basis of these results, it is proposed that increasing methyl group substitution results in decreased As sorption and increased As desorption on AAO.

Introduction

Arsenic originates in many rocks and minerals throughout the world. The weathering of these rocks and minerals releases As into the environment as inorganic species. The predominant oxidation states for inorganic As species are arsenate (As^V, H_3AsO_4) and arsenite (As^{III}, H_3AsO_3). In addition to inorganic forms, organic forms of As also exist in nature, typically occurring in terrestrial environments as MMA ($CH_3H_2AsO_3$) and DMA ($(CH_3)_2HAsO_2$). MMA and DMA have historically been used as herbicides and pesticides in agriculture (*1*). Due to cotton's tolerance to MMA, it was applied particularly to fields in the "cotton belt" of the United States, including Alabama, Arkansas, Texas, Louisiana, and Mississippi, to control weedy grasses (*1*). DMA was simultaneously applied as a defoliant. In the 1990s, more than 3000 t per year of MMA and more than 30 t per year of DMA were applied in cotton belt states (*2*). Subsequent studies on the surface water from these cotton producing regions have shown elevated levels of methylarsenates (*3*). MMA also has been used as a herbicide on golf courses, and it has been linked to elevated As concentrations in groundwater in southern Florida (*4*). Additionally, MMA has been used as a pesticide to control mountain pine beetle (*Dendroctonus ponderosae*) outbreaks in British Columbia, Canada (*5*). Approximately 960 kg of MMA were applied annually, and over 60 000 trees in the Cascades Forest District were treated with MMA between 2000 and 2004 (*6, 7*).

Arsenic has attracted large public interest due to its acute toxicity. Arsenic toxicity and the mode of toxin mechanisms depend on its speciation. Arsenite species, As^{III}, MMA^{III}, and DMA^{III}, are generally more toxic than arsenate species, As^V, MMA^V, or DMA^V (*8*). MMA and DMA are produced in many animals, including human beings via the methylation of arsenic. During the methylation processes, MMA^{III} and DMA^{III} are produced as intermediate products and are considered more toxic compounds than As^V or As^{III} (*8, 9*). Although MMA^V and DMA^V themselves possess lower toxicity than As^V or As^{III}, their reduction can produce very toxic MMA^{III} or DMA^{III}.

Aluminum oxides are ubiquitous in the environment and are one of the most important mineral oxides in soil systems. Unlike iron oxides, Al oxides are stable over a range of redox conditions. Under a reduced environment, Al oxides can influence contaminant transport to a larger extent than iron oxides can. Due to their reactivity and high surface area, AAOs have high sorption capacities for a range of environmental contaminants, including MMA^V and DMA^V. Synthetic analogues for AAOs can be used as a surrogate since natural AAOs are difficult to isolate from natural soils (*10*). To date, there has been no extensive investigation on methylarsenate sorption to Al oxides, including AAOs, employing molecular scale techniques. Accordingly, the goal of this study is to characterize MMA^V and DMA^V sorption to AAO, employing macroscopic and molecular scale techniques.

Materials and Methods

Detailed descriptions of the materials and methods are presented in the Supporting Information.

Arsenic Compounds. Reagent grades As^V, MMA, and DMA were used in this study. The molecular structures and pK_a of As^V, MMA, and DMA are shown in Figure S1 and Table S1.

Amorphous Aluminum Oxide Synthesis. AAO was synthesized by titrating an aluminum chloride solution with sodium hydroxide (*10*). The suspension was stored in a refrigerator at 4 °C and used in experiments within three weeks from the time of synthesis. XRD analysis confirmed that the oxide was amorphous. Nitrogen BET analysis revealed that the average surface area was 140 m^2/g.

Sorption Isotherm Studies. Sorption isotherms were determined via batch experiments at pH 5 and 7 with various As concentrations, ranging from 0.05 to 1.5 mM. Briefly, AAO suspensions (0.5 g/L), containing 0.01 M $NaNO_3$, were placed in 50 mL centrifuge tubes and equilibrated at pH 5 or 7 for 48 h with As^V, MMA, or DMA. Throughout the experiment, the pH of the solutions and samples was adjusted with 0.1 M HNO_3 or 0.1 M NaOH. The pH was measured and adjusted three times per day to maintain a pH of 5 or 7. The suspensions were centrifuged, and supernatants were sampled using syringe filters (Nylon 0.22 μm). The As concentrations were analyzed using inductively coupled plasma atomic emission spectroscopy (ICP-AES).

Sorption Kinetics Studies. Sorption kinetics experiments were conducted using a method similar to the sorption

* Corresponding author phone: (302) 831-1286; e-mail: mshimizu@udel.edu.

† Present address: Department of Land, Air, and Water Resources, University of California Davis, Davis, CA 95616.

10.1021/es9027502
Published on Web 12/16/2009

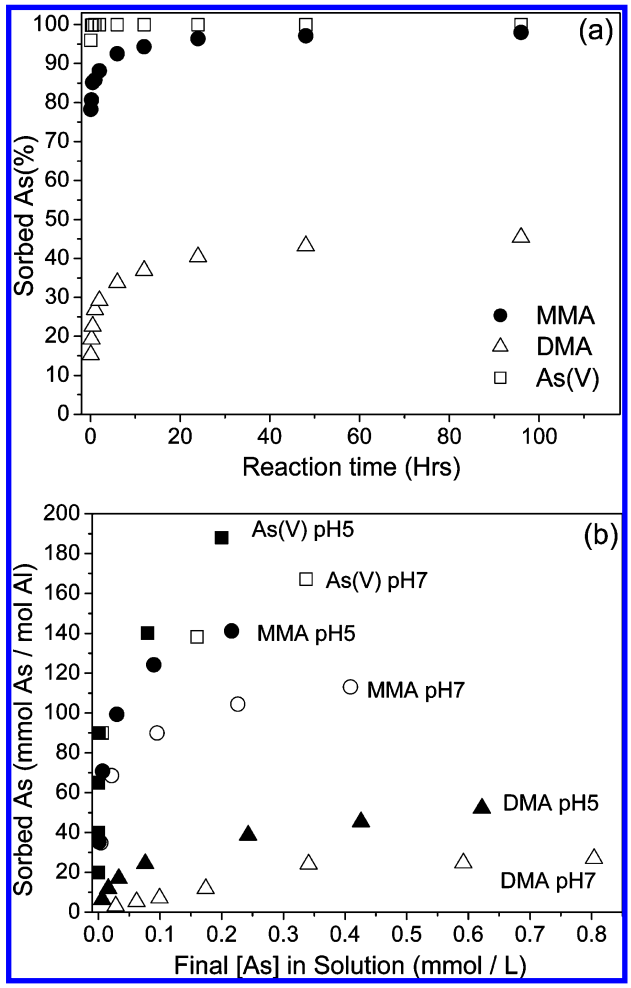

FIGURE 1. MMA, DMA, and As(V) sorption kinetics (a) and isotherms (b) on AAO.

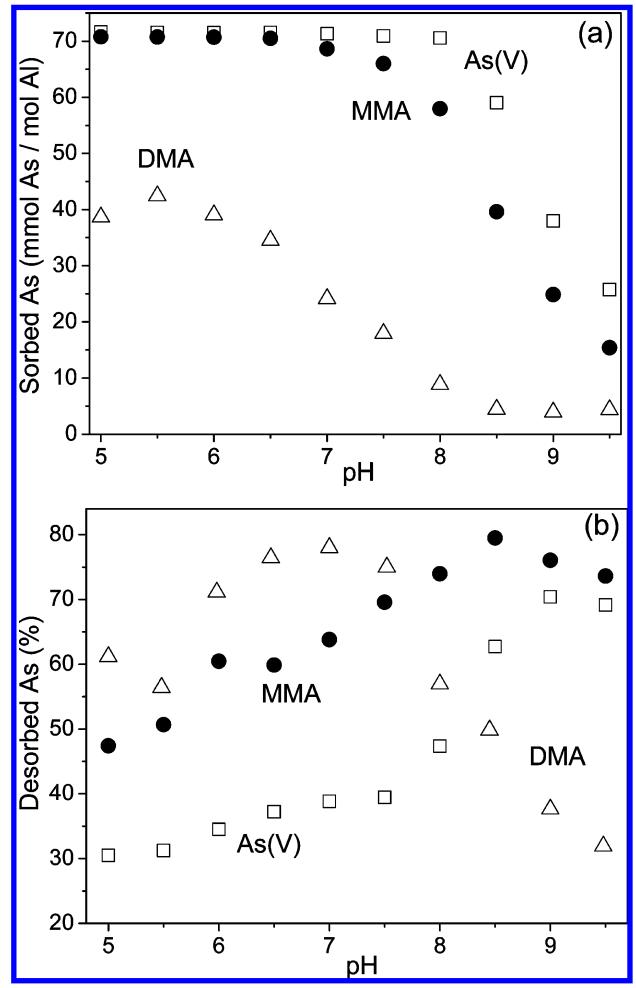

FIGURE 2. MMA, DMA, and As(V) sorption edges on AAO (a) and desorption from AAO (b).

isotherm study, employing 0.5 g/L AAO, and 0.5 mM As^V, MMA, or DMA, in 0.01 M $NaNO_3$ at pH 6 with 1 mM MES buffer. The samples were reacted for various time periods, ranging from 5 min to 96 h. The As concentrations were analyzed using ICP-AES.

Sorption Edge Studies. Sorption edge experiments were conducted using a method similar to the sorption isotherm studies. Briefly, AAO suspensions (0.5 g/L) with 0.01 M $NaNO_3$ were reacted with 0.5 mM MMA or DMA at various pH values, ranging from 5 to 9.5 for 48 h. The As concentrations were analyzed using ICP-AES.

Desorption Studies. Desorption studies were conducted by using phosphate as a desorbing agent. At the end of the sorption edge experiments, the suspension was centrifuged, and solution was replaced with phosphate (NaH_2PO_4) solution to achieve 0.05 M phosphate in each tube. The pH was adjusted and maintained so that the desorption pH was the same as the pH at the end of the sorption edge experiments. The samples were equilibrated for another 48 h, and the As concentrations were analyzed by ICP-AES.

Fourier Transform Infrared Spectroscopy (FTIR) Investigations. FTIR spectra were collected using a Thermo Nicolet Nexus spectrometer equipped with a singe bounce attenuated total reflectance (ATR) accessory with a diamond internal reflection element (SmartOrbit, Thermo) and MCT/A detector. A background electrolyte solution of 0.01 M NaCl was used instead of $NaNO_3$ to prevent any signal interference arising from NO_3^-. Aliquots of 100 μL each of MMA or DMA sorbed AAO suspension were deposited on the crystal, and 128 scans were collected at 4 cm^{-1} resolution. The 0.01 M NaCl and AAO spectra were collected at the same time and subtracted by using OMNIC Version 7.2. Aqueous phases of MMA and DMA were also subtracted from the spectra to account for unsorbed/solution phases.

X-ray Absorption Spectroscopy (XAS) Investigations. All XAS samples were prepared using similar experimental methods as those for the sorption edge experiments with an initial As concentration of 0.1 mM at pH 5 for all samples. After 48 h of reaction, samples were centrifuged and washed with 0.01 M $NaNO_3$ three times to remove excess As compounds. After the third centrifugation, the wet paste was kept moist by sealing the tubes and saving them for analysis. Arsenic K-edge (11 867 eV) XAS spectra were collected at X11A beamline at the National Synchrotron Light Source (NSLS) at Brookhaven National Laboratory. Three spectra per sample were collected, and the SIXPack/IFEFFIT program package was used to analyze the data (*11*). The inflection point of all samples did not change between the first and last scan. Final fitting of the spectra was conducted on Fourier transformed κ^3 weighted spectra in *R* space. During the fitting process, the coordination numbers for MMA and DMA, As−O and As−C, were fixed to reduce adjustable parameters. The molecular configurations of MMA and DMA sorbed to AAO based on XAS data analysis were created by using GaussView (*12*).

Results and Discussion

Sorption Kinetics Studies. Sorption kinetics experiments for As^V, MMA, and DMA on AAO revealed biphasic sorption characteristics; fast initial sorption was followed by slow continuous sorption (Figure 1a). As^V and MMA sorption were

nearly complete by the end of the 96 h experimental periods, but DMA sorption was not. As^V sorption reached a maximum before the first sample was collected (5 min). The data showed that the MMA sorption rate was slightly lower than the As^V sorption rate. 78% of added MMA was sorbed within the first 5 min, and rapid MMA sorption continued for 6 h at which time 92% of the initially added MMA was sorbed. MMA sorption reached pseudoequilibrium in 24 h. In contrast to As^V and MMA, only 15% of the added DMA was sorbed in 5 min. Rapid DMA sorption occurred during the first 6 h, and 34% of the initially added DMA was sorbed. DMA sorption reached pseudoequilibrium in 48 h, but only 45% of the added DMA was sorbed at the end of 96 h.

As^V, MMA, and DMA's molecular structural variations can explain the differences in sorption kinetics. The kinetics data showed As^V, with no methyl group substitution, had the highest sorption rate, while DMA, with two substituted methyl groups, had the lowest sorption rate. Increasing the methyl group substitution results in fewer hydroxyl groups being available for deprotonation and surface complex formation. On the basis of their pK_a values (Table S1) and the number of deprotonation sites, As^V has the largest quantity of negatively charged species, and DMA has the smallest quantity of negatively charged species at pH 5. Electrostatic attraction between positively charged AAO (Figure S2) and negatively charged As species is the highest for As^V and the lowest for DMA. In addition, if MMA and DMA form outer-sphere complexes similar to As^V, the electrostatic attraction can affect the complex formation and therefore impact the rate of sorption (*13, 14*). In the case of inner-sphere complex formation via sharing of oxygen, As^V can have six possible edge sites, MMA can have only three possible edge sites, and DMA can have only one edge site to form bidentate binuclear complexes with AAO. In the case of monodentate mononuclear complex formation, As^V can have four possible sites, MMA can have three possible sites, and DMA can have two possible sites. Less reactive sites can result in a lower probability of forming any surface complexes and increased time for aligning to a favorable molecular orientation, which could decrease the rate of sorption of MMA and DMA.

Sorption Isotherm Studies. Sorption isotherms for As^V, MMA, and DMA showed increasing As sorption at decreasing As sorption rates as the initial As^V, MMA, and DMA concentrations increased from 0.01 to 1 mM (Figure 1b). As^V, MMA, and DMA sorption were higher at pH 5 than at pH 7. Similar trends were observed for ferrihydrite (*15*). MMA sorption at pH 5 was as high as As^V sorption at the initial MMA concentrations below 0.75 mM. As the initial MMA concentration increased above 0.75 mM, a smaller percentage of the added MMA was sorbed to AAO compared to As^V sorption. At pH 7, almost 100% of the added MMA was sorbed to AAO at the initial MMA concentrations below 0.5 mM, and above this concentration a smaller percentage of the added MMA was sorbed. DMA sorption was much less than As^V and MMA sorption to AAO. At pH 5, DMA sorption reached approximately 85% of the initial DMA concentration (0.05 mM), and this sorption ratio decreased to 36% at the initial DMA concentration of 1 mM. At pH 7, approximately 40% of the initial DMA concentration (0.05 mM) was sorbed, and this sorption ratio decreased to approximately 20% at the initial DMA concentration of 1 mM. Compared to the MMA and DMA sorption isotherm study on ferrihydrite, sorption maxima values (Table S2) for MMA and DMA are comparable between AAO and ferrihydrite.

MMA and DMA sorption was higher at pH 5 than at pH 7 because the AAO surface was more positively charged at pH 5 than at pH 7 (Figure S2), resulting in stronger electrostatic attraction at pH 5 than pH 7. In addition, the charge differences between As species also influenced the higher sorption of As^V and lower sorption of DMA due to the larger quantity of negatively charged As^V and the smaller quantity of negatively charged DMA at any pH.

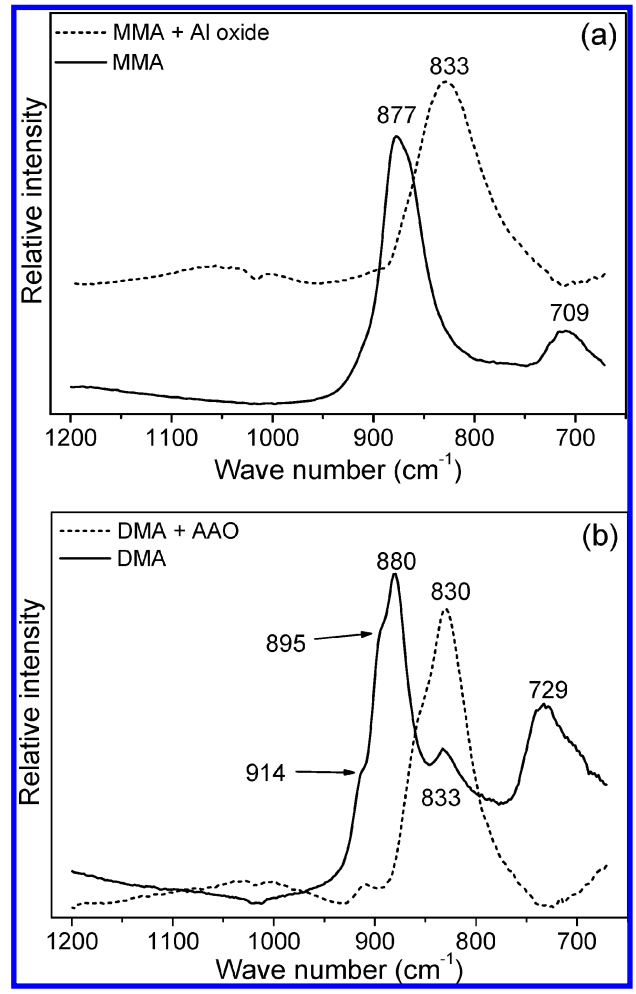

FIGURE 3. FTIR spectra for MMA and MMA sorbed on AAO (a) and DMA and DMA sorbed on AAO (b).

The differences in molecular structures also affected the sorption maximum. A methyl group substituted to an As atom makes the MMA molecule larger than As^V. For example, the average As−O distance is approximately 1.7 Å, and the average As−C distance is approximately 1.9 Å (*16, 17*). In addition, three hydrogen atoms are attached to the C atom with a typical H covalent bond distance of approximately 1 Å. This makes the As−O−H linear distance approximately 2.7 Å, and the As−C−H linear distance approximately 2.9 Å. The methyl groups also do not form hydrogen bonding within or with other molecules, while hydroxyl groups do. As a result, the number of MMA molecules that can cover and sorb to the AAO surface becomes smaller than that for As^V. DMA has an additional methyl group and a total of two methyl groups substituted for the As atom. The DMA molecule size is much larger than As^V. It is also possible that the second methyl group substitution magnified the factors discussed above.

pH Sorption Edge Studies. The general trend in pH sorption edges showed higher sorption at lower pH, and as the reaction pH increased, the sorption decreased (Figure 2a) similar to MMA and DMA sorption on ferrihydrite (*15*). MMA sorption was almost 100% at a pH value below 6.5. Sorption gradually decreased as pH increased above pH 6.5. At pH 9.5, approximately 20% of MMA was sorbed to AAO. MMA sorption was lower than As^V sorption above pH 6.5. DMA sorption behavior showed a parabolic sorption curve and was different from As^V and MMA with less DMA sorbed to AAO. DMA sorption increased from pH 5 to 5.5 where the maximum sorption occurred. Above pH 5.5, DMA sorption

TABLE 1. Structural Parameters for XAS Analysis of MMA and DMA Solutions and MMA and DMA Sorbed on AAO

	MMA	MMA−Al	DMA	DMA−Al	As^V−Al[g]
As−O					
CN[a] (fixed)	3	3	2	2	
R^b (Å)	1.69 ± 0.004[f]	1.69 ± 0.007	1.69 ± 0.008	1.70 ± 0.01	
Σ^{2c} (Å^2)	0.0027 ± 0.0003	0.0012 ± 0.0006	0.0026 ± 0.0005	0.0011 ± 0.0004	
As−C					
CN (fixed)	1	1	2	2	
R (Å)	1.88 ± 0.09	1.89 ± 0.008	1.90 ± 0.011	1.90 ± 0.01	
Σ^2 (Å^2)	0.0015 ± 0.0008	0.0009 ± 0.0025	0.0014 ± 0.0008	0.0013 ± 0.0007	
As−Al					
CN		2.1 ± 0.94		2.4 ± 0.6	1.3−2.2
R (Å)		3.16 ± 0.022		3.17 ± 0.01	3.11−3.19
Σ^2 (Å^2)		0.0058 ± 0.0017		0.0056 ± 0.0015	0.0009−0.007
$E_0{}^d$ (eV)	4.88 ± 0.82	4.43 ± 0.93	6.15 ± 1.57	4.70 ± 1.11	
$S_0{}^{2e}$ (fixed)	0.98	0.98	0.98	0.98	

[a] Coordination number. [b] Interatomic distance. [c] Debye−Waller factor. [d] Energy shift. [e] Amplitude reduction factor. [f] Standard deviation. [g] Selected references of As^V sorbed on aluminum oxides analyzed by EXAFS (*16, 27, 28*).

decreased as pH increased. At pH 5.5, approximately 60% of DMA was sorbed to AAO. Above pH 8, only a small percentage of DMA was sorbed to AAO.

AAO has a point of zero charge at pH ≈ 9 (Figure S2). Below this pH, electrostatic attraction enhanced sorption. As pH increased, the AAO surface became less positive. Decreases in electrostatic attraction diminished As^V, MMA, and DMA sorption, and less sorption at high pH was attributed to increasing repulsive potentials between the negatively charged As species and the negatively charged AAO surfaces (*15*). The charge differences between As species also influenced the higher sorption of As^V and lower sorption of DMA. Electrostatic attraction also helps to explain the pH where maximum DMA sorption occurred. Typically, sorption maxima are observed at pH values near the pK_a values for oxyanions; however, the sorption maximum for DMA on AAO was observed at pH 5.5, which is lower than its pK_a of 6.14 (*18*). The shift in sorption maximum pH is attributed to the AAO surface charge. At lower pH, the AAO surface is more positively charged (Figure S2) and can enhance electrostatic attraction between AAO and DMA. Similar trends were observed for DMA sorption on goethite (sorption maximum at pH below 6) and As^{III} sorption on γ-aluminum oxide (sorption maximum at pH below pK_a = 9.22) (*15, 16*).

Desorption Studies. Complete MMA and DMA desorption by phosphate was not observed over the pH ranges examined (Figure 2b). The desorption ratio was calculated as desorbed As to sorbed As (desorbed As/sorbed As) %. As^V, MMA, and DMA desorption envelopes showed a similar trend. Arsenic desorption increased as pH increased until a particular pH, and further pH increases resulted in decreased desorption. As^V desorption increased as pH increased until pH 9. At pH 5 and 9, 31% and 70% of sorbed As^V was desorbed, respectively. Above pH 9, As^V desorption decreased as pH increased. MMA desorption increased until pH 8.5, and as pH increased above pH 8.5, desorption decreased. At pH 5, 47% of sorbed MMA was desorbed, and the ratio increased up to 80% at pH 8.5. DMA desorption increased from pH 5 to 7 and decreased above pH 7. At pH 5 and 7, 61% and 78% of sorbed DMA were desorbed, respectively. Desorption decreased to 32% at pH 9.5. Compared to the desorption study on ferrihydrite, the trend in desorption is similar with DMA desorbing the most and As^V the least (*15*).

The increases in desorption at lower pH indicated that sorption occurred partially via electrostatic attraction. As pH increased, the AAO surface became less positive, weakening the attraction, resulting in phosphate being able to replace sorbed As. The desorption decreased at higher pH because less As^V, MMA, and DMA were sorbed initially and less As was desorbed by phosphate due to its strong affinity to AAO. Similar to As^V desorption from γ-aluminum oxide, a portion of MMA and DMA sorption was irreversible (*19*). The binding of MMA, DMA, and As^V to AAO is fairly strong, as evidenced by the inability of phosphate to desorb the As species. This suggests that MMA, DMA, and As^V form similar surface complexes with AAO, such as inner-sphere complexes, since the inner-sphere complex formation leads to irreversible sorption (*18*).

FTIR Investigations. At pH 5, the dominant form of MMA (pK_{a1} = 4.19) is $CH_3AsO_2OH^{-1}$ and DMA (pK_a = 6.14) is $(CH_3)_2AsOOH$. The MMA aqueous solution spectrum had peaks at 877 and 709 cm^{-1}, corresponding to $\nu_s(AsO_2)$ and ν(As−OH), respectively (Figure 3a) (*20–22*). Peaks from a methyl group, such as those observed in the DMA FTIR spectra, were not observed in the MMA spectra. This is likely due to the weak peak signal from a single methyl group being overshadowed by the intense $\nu_s(AsO_2)$ peak (*22*). When MMA was sorbed to AAO, the peak at 877 cm^{-1} shifted down to 833 cm^{-1}, and the peak at 709 cm^{-1} disappeared. This could be due to an apparent increase in molecular symmetry upon the sorption or to the peak shifting to a lower wavenumber (<650 cm^{-1}) below the wavenumber limit for the MCT/A detector. Due to decreased signal sensitivity, the DTGS detector was unable to provide good quality data for examination of lower wave numbers. The DMA aqueous spectrum contained two shoulders at 914 and 895 cm^{-1} and three peaks at 880, 833, and 729 cm^{-1} (Figure 3b). These shoulders and peaks were assigned as $\rho(CH_3)$, $\rho(CH_3)$, ν(As−O), $\nu(As-O_2^-)$, and ν(As−OH), respectively (*21–23*). When DMA was sorbed to AAO, the peak at 880 cm^{-1} shifted down to 830 cm^{-1} (overlapping the previous peak at 833 cm^{-1}), the peak at 729 cm^{-1} disappeared, and the shoulder at 914 cm^{-1} did not shift. This also could be due to an apparent increase in molecular symmetry upon the sorption or to the peak shifting to a lower wavenumber (<650 cm^{-1}).

The observed peak shifts were likely caused by inner-sphere complex formation and changes in the vibrational freedom of MMA and DMA upon sorption to AAO. During this process, one or two of the As−O(H) groups from MMA or DMA may go through ligand exchange reactions with OH groups from the AAO surface, forming inner-sphere complexes. As^V sorption to ferrihydrite and AAO showed similar As−O peak shifts to lower wave numbers (*24*). Similarly, As^V has been shown to form inner-sphere complexes with iron and aluminum oxides (*16, 24, 25*). During As^V sorption on AAO, the As−O peak (945 cm^{-1}) downshifts to 862 cm^{-1} as a result of inner-sphere complex formation at the mineral surface (*24*). MMA's and DMA's As−O peak shifts were similar

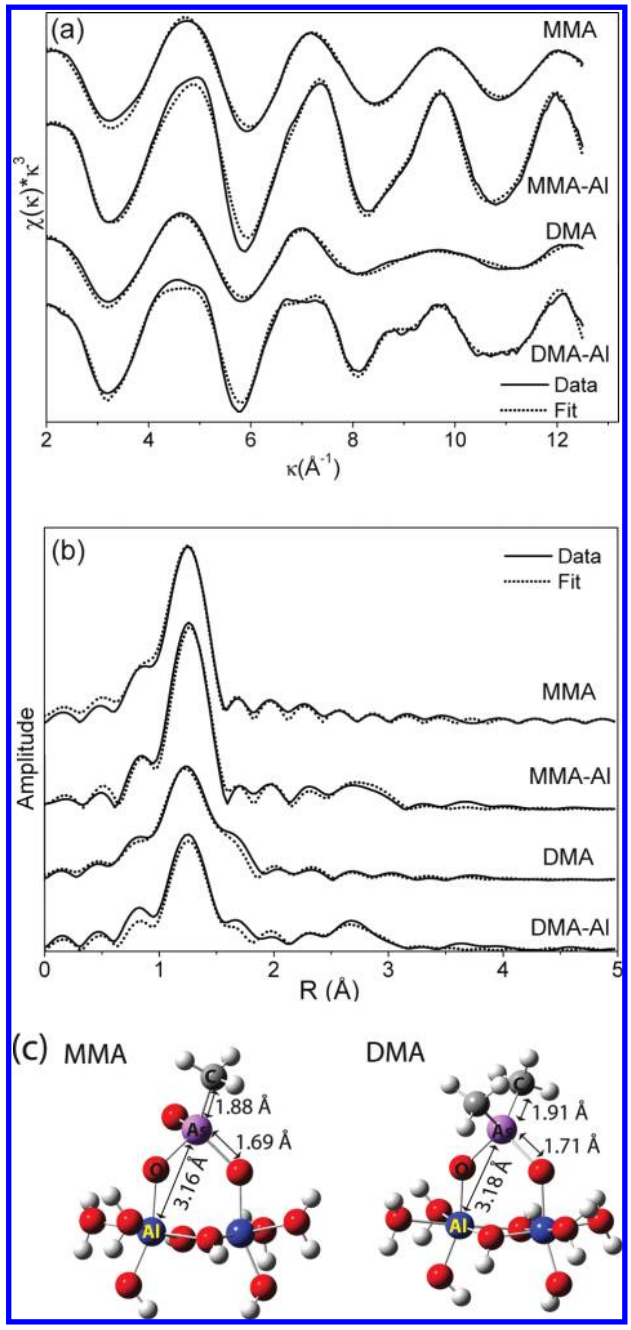

FIGURE 4. MMA and DMA XAS spectra in κ space (a), Fourier transformation of XAS spectra (b), and molecular configurations of MMA and DMA sorbed on AAO cluster (c).

to the As^V peak shift, which suggested that MMA and DMA also formed inner-sphere complexes with AAO. In addition, the shoulder peak at 914 cm^{-1}, representing the methyl groups of DMA, did not shift upon the addition of AAO to the solution, indicating that the methyl groups were not involved in DMA−AAO surface complex formation.

XAS Investigations. On the basis of the fit for MMA sorption on AAO, the As−O bond distance was calculated to be 1.69 Å, while the As−C bond distance was 1.89 Å, and 2.1 aluminum atoms were located at an As−Al interatomic distance of 3.15 Å (Table 1). As−O and As−C bond distances from this study agreed with other experimental studies and XAS investigations (*21, 26*). The coordination number and As−Al distances were indicative of a MMA−AAO bidentate binuclear complex (Figure 4c) (*16, 27, 28*). On the basis of the coordination number and bond distance (Table 1), DMA also formed a bidentate binuclear complex with AAO (Figure 4c). It should be mentioned that it is possible that MMA and DMA also form outer-sphere complexes with AAO, similar to As^V sorption on aluminum and iron oxides; however, XAS and FTIR techniques used in this study cannot verify outer-sphere complex formation (*13*).

Our results showed that MMA and DMA formed bidentate binuclear complexes on AAO, similar to As^V (*16, 27, 28*). This result partially agrees with another MMA and DMA XAS study where MMA formed a bidentate binuclear complex and DMA formed a monodentate mononuclear complex on nanocrystalline titanium oxide (TiO_2) (*26*). One possible explanation for DMA bidentate binuclear complexation with AAO could be the surface charge differences between AAO and TiO_2. TiO_2 had a PZC of pH 5.8, and the XAS sample pH in the study of Jing et al. (2005) was 5, while in this study AAO had a PZC of pH 9 and the reaction pH was 5. At pH 5, the TiO_2 surface is more neutrally charged, and the AAO surface is more positively charged. There are many protonated $Al-OH_2^+$ functional groups on the AAO surface. The O atom in the $Al-OH_2^+$ group shares electrons with the second proton, and the electron density of the O atom is shifted toward protons. Because the O atom has high electron negativity, it tends to pull the electron density between Al and O closer to the O atom to fulfill its charge. This makes the Al atoms in $Al-OH_2^+$ more positively charged overall, compared to that of Al−OH. In addition, $Al-OH_2^+$ has a higher water exchange rate than a neutral Al−OH surface. As a result, $Al-OH_2^+$ functional groups can have a higher potential to trigger ligand exchange reactions with As−O or As−OH from the DMA to form a bidentate binuclear complex.

However, these observations do not explain differences in the sorption/desorption characteristics between As^V, MMA, and DMA. One can assume that if all three species formed the same type of surface complex, the sorption/desorption capacity would be similar, but this was not the case in this study. This discrepancy seems to arise from differences in molecular structure, rather than different types of surface complex formation. As discussed earlier, more methyl groups attached to the As atom can lead to less affinity of the As species for the AAO surface. Another reason for the lower sorption affinity of DMA on the AAO surface is that the formation of bidentate binuclear complexes may put stress on the geometry of DMA. Such steric hindrances can make this type of surface complex formation more unstable.

In the DMA molecule, two oxygen atoms are attached to an As atom (Figure S1). One of the oxygen atoms forms a π bond with the As atom, As═O, and another oxygen atom is within a hydroxyl (OH) group bound to As, As−OH. The formation of a bidentate binuclear complex between DMA and the AAO surface requires that both As═O and As−OH bonds are involved in the complexation. The As═O bond becomes an As^+-O^- bond and another oxygen atom from the As−OH forms a complex with an Al atom on the oxide surface. On the basis of the XANES spectrum of DMA sorbed on AAO, the oxidation state of the As remains pentavalent (Figure S3), and the inflection points of free DMA and sorbed DMA are consistent with other studies (*26, 29*). To maintain the oxidation state, additional negative charge has to be supplied to the As atom. Methyl groups may provide a small amount of additional negative charge by being closer to the As atom. However, due to the size and the protons attached to the C atoms, two methyl groups are unlikely to move closer to the As atom to satisfy all the missing charge. Instead, O atoms, forming a bidentate binuclear complex, may move closer to the As atom to fulfill the remaining charge imbalance. This can make the Al−O complexation weaker than a typical bidentate binuclear complex and result in large DMA desorption when the complex is replenished by phosphate.

Environmental Significance. MMA and DMA are generally minor components of total As in the environment but can sometimes reach 10−50% of total As (*3, 30, 31*). A better understanding of MMA and DMA sorption on AAO, an important soil component analogue, is critical to predict the fate of these chemicals in the environment. Our study revealed that MMA and DMA sorption on AAO showed similar trends to As^V sorption on AAO with slightly lower MMA sorption and much lower DMA sorption than As^V sorption. FTIR and XAS studies revealed that MMA and DMA formed bidentate binuclear complexes, similarly to As^V sorption on aluminum oxides. These findings suggest that the more mobile MMA and DMA can easily percolate to groundwater or be taken up by plants compared to As^V. More mobile, and therefore more bioavailable, MMA and DMA can be demethylated to As^V or As^{III}. Accordingly, MMA and DMA sorption can play an important role in total arsenic cycling in the environment. MMA and DMA sorption mechanisms, along with sorption envelope results, are also useful for establishing important parameters for surface complexation model development.

Acknowledgments

We would like to thank Cathy Olsen at the University of Delaware for assistance with the ICP-AES analyses samples and Pandya Kumi at NSLS beamline X11A for help with XAS data collection. We are also grateful to three anonymous reviewers for their constructive suggestions.

Supporting Information Available

Detailed materials and methods section, MMA and DMA molecular structure (Figure S1), electrophoretic mobility study (Figure S2), MMA and DMA XANES spectra (Figure S3), pK_a values for MMA and DMA (Table S1), and Langmuir equation parameters (Table S2). This material is available free of charge via the Internet at http://pubs.acs.org/.

Literature Cited

(1) Dickens, R.; Hiltbold, A. E. Movement and persistence of methanearsonates in soil. *Weeds* **1967**, *15* (4), 299–304.
(2) Perkins, H. H.; Brushwood, D. E. Effects of mechanical processing and wet treatments on arsenic acid desiccant residues in cotton. *Text. Chem. Color.* **1991**, *23* (2), 26–28.
(3) Bednar, A. J.; Garbarino, J. R.; Ranville, J. F.; Wildeman, T. R. Presence of organoarsenicals used in cotton production in agricultural water and soil of the southern United States. *J. Agric. Food Chem.* **2002**, *50* (25), 7340–7344.
(4) Feng, M.; Schrlau, J. E.; Snyder, R.; Snyder, G. H.; Chen, M.; Cisar, J. L.; Cai, Y. Arsenic transport and transformation associated with MSMA application on a golf course green. *J. Agric. Food Chem.* **2005**, *53* (9), 3556–3562.
(5) Albert, C. A.; Williams, T. D.; Morrissey, C. A.; Lai, V. W. M.; Cullen, W. R.; Elliott, J. E. Dose-dependent uptake, elimination, and toxicity of monosodium methanearsonate in adult zebra finches (Taeniopygia guttata). *Environ. Toxicol. Chem.* **2008**, *27* (3), 605–611.
(6) Morrissey, C. A.; Dods, P. L.; Albert, C. A.; Cullen, W. R.; Lai, V. W.-M.; Williams, T. D.; Elliot, J. E. *Assessing forest bird exposure and effects from Monosodium Methanearsonate (MSMA) during the Mountain Pine Beetle epidemic in British Columbia*; Technical Report Series No. 460; Environment Canada, Pacific and Yukon Region, Delta, British Columbia, 2006.
(7) Dost, F. *Public health and environmental impacts of monosodium methanearsonate as used in bark beetle control in British Columbia*; FS 48 HIS 95/2 Ministry of Forests: Victoria, BC, Canada, 1995.
(8) Styblo, M.; Del Razo, L. M.; Vega, L.; Germolec, D. R.; LeCluyse, E. L.; Hamilton, G. A.; Reed, W.; Wang, C.; Cullen, W. R.; Thomas, D. J. Comparative toxicity of trivalent and pentavalent inorganic and methylated arsenicals in rat and human cells. *Arch. Toxicol.* **2000**, *74* (6), 289–299.
(9) Petrick, J. S.; Ayala-Fierro, F.; Cullen, W. R.; Carter, D. E.; Aposhian, H. V. Monomethylarsonous acid (MMA(III)) is more toxic than arsenite in Chang human hepatocytes. *Toxicol. Appl. Pharmacol.* **2000**, *163* (2), 203–207.
(10) Goldberg, S.; Lebron, I.; Suarez, D. L.; Hinedi, Z. R. Surface characterization of amorphous aluminum oxides. *Soil Sci. Soc. Am. J.* **2001**, *65* (1), 78–86.
(11) Webb, S. M. SIXpack: a graphical user interface for XAS analysis using IFEFFIT. *Phys. Scr.* **2005**, *T115*, 1011–1014.
(12) Dennington, II, R.; Keith, T.; Millam, J.; Eppinnett, K.; Hovell, W. L.; Gilliland, R. *GaussView, Version 3.09*; Semichem, Inc.: Shawnee Mission, KS, 2003.
(13) Catalano, J. G.; Park, C.; Fenter, P.; Zhang, Z. Simultaneous inner- and outer-sphere arsenate adsorption on corundum and hematite. *Geochim. Cosmochim. Acta* **2008**, *72* (8), 1986–2004.
(14) Sposito, G. The operational definition of the zero-point of charge in soils. *Soil Sci. Soc. Am. J.* **1981**, *45* (2), 292–297.
(15) Lafferty, B. J.; Loeppert, R. H. Methyl arsenic adsorption and desorption behavior on iron oxides. *Environ. Sci. Technol.* **2005**, *39* (7), 2120–2127.
(16) Arai, Y.; Elzinga, E. J.; Sparks, D. L. X-ray absorption spectroscopic investigation of arsenite and arsenate adsorption at the aluminum oxide-water interface. *J. Colloid Interface Sci.* **2001**, *235* (1), 80–88.
(17) Trotter, J.; Zobel, T. Stereochemistry of arsenic 0.16. Cacodylic acid. *J. Chem. Soc.* **1965**, (AUG), 4466–4471.
(18) Sparks, D. L. *Environmental Soil Chemistry*, 2nd ed.; Academic Press: Boston, 2002.
(19) Arai, Y.; Sparks, D. L. Residence time effects on arsenate surface speciation at the aluminum oxide-water interface. *Soil Sci.* **2002**, *167* (5), 303–314.
(20) Vansant, F. K.; Vanderveken, B. J.; Herman, M. A. Vibrational analysis of methylarsonic acid, trideuteromethylarsonic acid and their anions. *J. Mol. Struct.* **1976**, *35* (2), 191–200.
(21) Grundler, H. V.; Schumann, H. D.; Steger, E. Raman and infrared spectroscopic investigation of alkyl derivatives of arsenic acid 0.6. AsO bond—calculation of force constants and vibrational energy-distribution in compounds of type $RAsO_3X_2$ and R_2AsO_2X. *J. Mol. Struct.* **1974**, *21* (1), 149–157.
(22) Cowen, S.; Duggal, M.; Hoang, T.; Al-Abadleh, H. Vibrational spectroscopic characterization of some environmentally important organoarsenicals - A guide for understanding the nature of their surface complexes. *Can. J. Chem.* **2008**, *86*, 942–950.
(23) Vansant, F. K.; Vanderve, Bj; Herman, M. A. Vibrational analysis of dimethylarsinic acid. *Spectrochim. Acta, Part A* **1974**, *A 30* (1), 69–78.
(24) Goldberg, S.; Johnston, C. T. Mechanisms of arsenic adsorption on amorphous oxides evaluated using macroscopic measurements, vibrational spectroscopy, and surface complexation modeling. *J. Colloid Interface Sci.* **2001**, *234* (1), 204–216.
(25) Waychunas, G. A.; Rea, B. A.; Fuller, C. C.; Davis, J. A. Surface-chemistry of ferrihydrite: Part 1. EXAFS studies of the geometry of coprecipitated and adsorbed arsenate. *Geochim. Cosmochim. Acta* **1993**, *57* (10), 2251–2269.
(26) Jing, C. Y.; Meng, X. G.; Liu, S. Q.; Baidas, S.; Patraju, R.; Christodoulatos, C.; Korfiatis, G. P. Surface complexation of organic arsenic on nanocrystalline titanium oxide. *J. Colloid Interface Sci.* **2005**, *290* (1), 14–21.
(27) Ladeira, A. C. Q.; Ciminelli, V. S. T.; Duarte, H. A.; Alves, M. C. M.; Ramos, A. Y. Mechanism of anion retention from EXAFS and density functional calculations: Arsenic (V) adsorbed on gibbsite. *Geochim. Cosmochim. Acta* **2001**, *65* (8), 1211–1217.
(28) Beaulieu, B. T.; Savage, K. S. Arsenate adsorption structures on aluminum oxide and phyllosilicate mineral sufaces in smelter-impacted soils. *Environ. Sci. Technol.* **2005**, *39* (10), 3571–3579.
(29) Smith, P. G.; Koch, I.; Gordon, R. A.; Mandoli, D. F.; Chapman, B. D.; Reimer, K. J. X-ray absorption near-edge structure analysis of arsenic species for application to biological environmental samples. *Environ. Sci. Technol.* **2005**, *39* (1), 248–254.
(30) Braman, R. S.; Foreback, C. C. Methylated forms of arsenic in environment. *Science* **1973**, *182* (4118), 1247–1249.
(31) Marin, A. R.; Pezeshki, S. R.; Masschelen, P. H.; Choi, H. S. Effect of dimethylarsenic acid (DMAA) on growth, tissue arsenic, and photosynthesis of rice plants. *J. Plant Nutr.* **1993**, *16* (5), 865–880.

ES9027502